URSI GASS 2020, Rome, Italy, 29 August - 5 September 2020

STDCC radar at 24 GHz: first measurement trials

André Sardo[(1)(2)], João R. Reis[(1)(2)], Luis Duarte[(1)(2)], Nuno Leonor[(1)(2)], Carlos Ribeiro[(1)(3)] and Rafael F. S. Caldeirinha[(1)(2)].
(1) Polytechnic Institute of Leiria, Leiria, Portugal
(2) Instituto de Telecomunicações - Leiria, Portugal
(3) TWEVO *Lda.*, Coimbra, Portugal

Abstract

This paper presents the first measurement trials for performance assessment of a real-time and high resolution monostatic radar operating at 24 GHz. The proposed real-time radar, which operates based on the sliding correlation of pseudo-noise (PN) sequences, provides a high time resolution better than 4 ns, useful for moving target identification (MTI) in the presence of highly dense clutter, under harsh environments and severe weather conditions (fog, snow and fire smoke or plume). The STDCC radar target detection capability is demonstrated in this paper, by measuring and identifying the radar data for 4 distinct scenarios, composed of multiple targets (up to 8), inside an anechoic chamber, demonstrating the potential of the proposed radar architecture.

1 Introduction

Radar technology has been used for many years, but its constant evolution is a demand due to the intensive interest of automotive and drone industry, to assist in autonomous driving and collision avoidance. To date, many radar topologies have been presented in the literature [1], but mostly are based on Frequency Modulated Continuous Wave (FMCW) technique. This technique, however, shows limited performance in heavy cluttered environments, where interference from other radars or communications may significantly degrade the radar's detection capability. Alternatively, Orthogonal Frequency Division Multiplexing (OFDM) is being proposed in [1, 2], to overcome the FMCW limitations. Nevertheless, the OFDM-based radars require high computational resources typically available in Field-Programmable Gate Array (FPGA) based architectures, in addition to expensive analogue-to-digital converters (ADC), making its implementation both inefficient and cost prohibitive for mass production. On the other hand, radar signal processing based on all-digital pseudo-noise (PN) sequences represents a quantum leap in future radar front-end architecture, presenting significant advantages in terms of low baseband computational demands and yielding a plethora of opportunities for massive deployment applications, *e.g.* autonomous driving scenario.

With this mindset, it is presented in this paper the first trails on a Swept Time-Delay Cross-Correlator (STDCC) PN Radar at 24 GHz. The proposed radar architecture, being described in this paper, follows the STDCC principle well covered in [3–6] and it is sought to mitigate incumbent and mutual interference risks, given its excellent autocorrelation properties. The experimental results included in this paper, demonstrate the potential of the proposed technique by clearly detecting and identifying 8 distinct metallic targets at 24GHz.

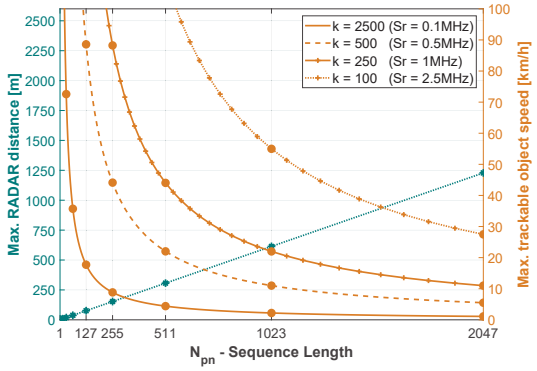

Figure 1. STDCC radar: maximum unambiguous distance and trackable object speed *vs.* N_{pn} sequence length, for a F_{tx} = 250MHz.

This paper is organised as follows: section 2 gives details about the proposed STDCC radar architecture, including a brief summary of the STDCC principle, the baseband signal generation in the digital domain, and finally, the radar architecture, including RF and IF stages. In section 3, the practical setup and the measurements scenarios are being described followed by a critical analysis of the experimental results. Finally, the main conclusions are drawn in section 4.

2 STDCC radar architecture

2.1 Radar principle

The STDCC PN radar proposed herein, explores the autocorrelation properties of PN sequences [3–6], particularly those of the type of maximal length. In this monostatic

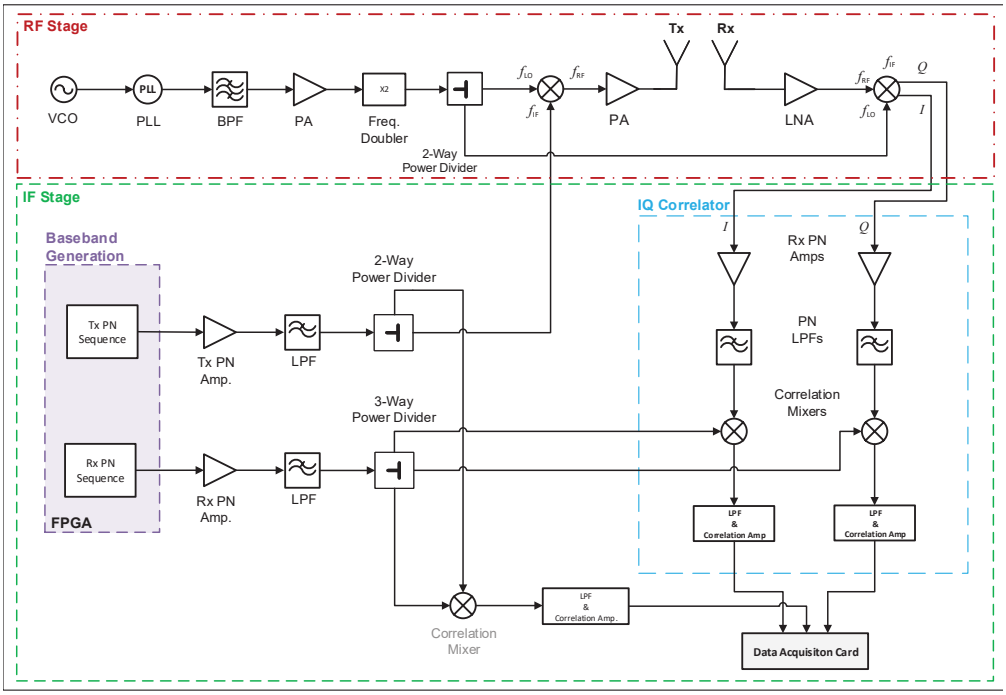

Figure 2. Block diagram of the STDCC radar architecture.

configuration (Fig. 2), two similar PN sequences are generated in the baseband of which, one is transmitted through the radio channel and the other shared directly with the receiver. At the receiver end, both PN sequences are correlated against each other to extract the radar channel information. Since both PN sequences are generated at two different rates, they 'slide' against each other in the time domain, effectively spreading (time-dilating) the multipath (or several target echoes) components out in time, at the output of the correlator. Thus, the maximum theoretical unambiguous distance for a target object to be detected, in metres, only depends on the PN sequence length (N_{pn}) and on the chip frequency (F_{tx}), while the maximum trackable object speed is set by frequency difference between the two generated sequences, denominated of slip-rate (Sr). In Fig. 1 it is presented the maximum theoretical unambiguous distance for the STDCC radar, for various N_{pn} sequences length and slip-rate settings. This is sought to provide the radar with high agility to adapt itself to different application scenarios, *e.g.* short and long range.

2.2 Baseband generation

The radar baseband generation, where PN sequences are being generated, is a subpart of the IF stage of the proposed radar architecture depicted in Fig. 2. In particular, a Xilinx Kintex-7 KC705 FPGA [7] has been used to generate the receiver and transmitter PN sequences. Real-valued bipolar maximum length PN binary sequences with $N_{pn} = 511$ points are generated in the FPGA and then outputted in its unipolar digital pins, with 250.1 MHz and 250 MHz clocks (Sr = 100 kHz), for the transmitter (Tx) and receiver (Rx), respectively. This technique allows the creation of an analogue baseband signal and eliminates the need for expensive high-speed Digital-to-Analogue Converters (DAC) daughter boards. The physical implantation baseband generation in algorithm and is explained with more detail in [6].

2.3 RF and IF architectures

The RF stage initiates in a high precision Voltage Controlled Oscillator (VCO) controlling a Phase-Locked Loop (PLL) to output the necessary 24 GHz. This, in turn is divided to source both mixers to up-convert and down-convert the baseband signal (IF). At the Tx mixer, the resulting signal is amplified to appropriate output power levels up to the limits of interest for the radar. At receiving end, the Rx mixer demodulates the channel radio signal into a differential signal with In-phase (I) and In-quadrature (Q) components, feeding into the IQ correlator block in the IF stage. *X-Microwave* technology was employed to achieve the mentioned RF stage (front-end) of the radar, allowing fast prototyping with their modular building block ecosystem for microwave components. The antennas used for this system were two identical 20 dB gain horn antennas (*Flann* 22240-20), located side-by-side.

In the IF stage, both I and Q received components are amplified and filtered before being fed into the correlation mixers, where the correlation is performed with the Rx PN sequence as previously mentioned in section 2.2. Further signal conditioning is performed in order to be properly captured by an ordinary data acquisition card (*Picoscope* 3406-D MSO). Besides the I and Q acquisition of the received signal, the correlation result between a copy of both

receiver and transmitter sequences is also acquired, in order to obtain clear temporal reference. These signals were then processed in real-time to estimate the targets distance and obtain a plan-position-indication (PPI), as it will be discussed next section.

3 Radar performance evaluation

3.1 Experimental setup

In order to assess the performance of the proposed radar, four distinct scenarios were assembled inside an anechoic chamber, in a 1-pole, 2-pole, 7-pole and 8-pole configuration, respectively. These scenarios were prepared to assess the radar's ability to detect targets in close proximity. The poles are composed of metal with 6 cm of diameter and 2 m of height, and are disposed inside a 6x5x2 m anechoic chamber, as indicated Fig. 3a. The radar was placed on top on a motorised rotating table, in the centre of the chamber, and it was made to rotate around its vertical axis. For all geometries, the radar system under test was made to rotate 360° with a 0.5° steps increment. For every angular step, 20 radar acquisitions have been measured, averaged (Power Delay Profile) and processed to obtain a PPI and assess the target identification performance. After processing, the results are then displayed in two different graph types: waterfall and polar plot, as depicted in Figs. 4 and 5, respectively. The waterfall plots represent the measured average PDP, where the x-axis corresponds to each measured azimuth angle and the y-axis corresponds to the detected radar distance. The polar plot depicts all detected peaks, at every angle, after applying a simple peak-detection algorithm.

3.2 Experimental results

The first measurement scenario considered a single metallic pole placed 1 m apart of the proposed radar aperture at boresight direction, where $\theta = 0°$ (Fig. 3a). According to the results, depicted in Fig. 4a and Fig. 5a, it is possible to observe the single target to be accurately detected by the STDCC radar. The target peak is correctly being identified inside the anechoic chamber at 1 m distance and at 0° in the boresight direction of the radar aperture, which is clearly visible in Fig. 5a. The colour variation gradient visible in the result occurs due to the radiation pattern of the antennae, which exhibits a half-power beam-width of around 23°, in both azimuth and elevation planes, at the considered frequency.

The second set of measurements was performed by adding an extra pole at a distance of 1.6 m and steered off 10° from the boresight direction ($\theta = 10°$), to the previous scenario. As depicted in Fig. 4b, both targets are also being detected and, in fact, they can be easily distinguished from each other. The estimated distances of both poles are confirmed by the polar plot of Fig. 5b, at $\theta = 0°, d = 1$m for the first target and at $\theta = 10°, d = 1.6m$, for the second target, corresponding to their real physical position inside the chamber.

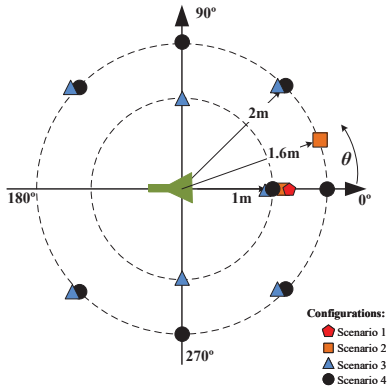

(a)

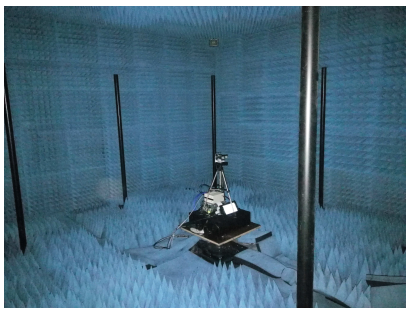

(b)

Figure 3. Experimental setup: (a) scenario setup for benchmarking and, (b) photography inside anechoic chamber.

For the third scenario, 7 poles were placed in an alternating fashion, at 1 m and 2 m apart of the radar with 45° increments starting from $\theta = -135°$. The proper detection of all 7 targets is visible in Fig. 4c. The correct angles of detection can be seen in Fig. 5c, as each pole is detected at the angles of $\theta = -135°, -90°, -45°, 0°, 45°, 90°$ and 135°. Although a few artefacts can be observed in the vicinity of the poles located at 1 m apart from the radar, these are still located well within the the spacial resolution of the radar.

As for the last scenario, Fig. 4d clearly shows the correct detection of all targets, where the 7 poles are located at 2 m apart at the same angles as the previous scenario and a single pole placed at 1 m apart at the angle $\theta = 0°$, including the same artifacts as the previous scenario. Most notably, the target placed at $\theta = 0°$ and 2 m further away is also being detected, despite of the fact it is masked by the first pole (no direct line of sight). Although the angle of this pole is being detected as being at around 7° in Fig. 5d, due to the *shadowing* of the pole at 1 m, the remaining poles detection was performed successfully.

For all the results presented, a maximum range error of only 9 cm between the reported distance and the effective physical distance have been detected. This error is acceptable, as it falls within the spacial precision associated with the used radar bandwidth. The signal level difference of around 7-9 dB between the poles depicted in Fig. 4b occurs due to the excess path loss corresponding to the travel distance

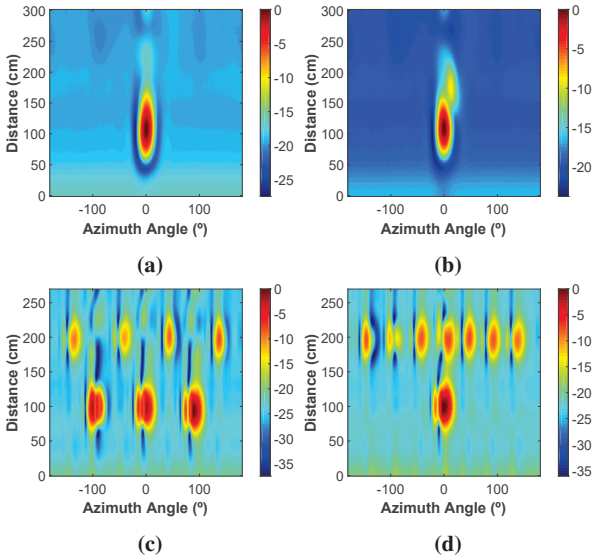

Figure 4. Waterfall PPI - normalised gain (in dB) *vs.* scanning angle, for: (a) 1-pole (b) 2-pole (c) 7-pole and (d) 8-pole, scenario.

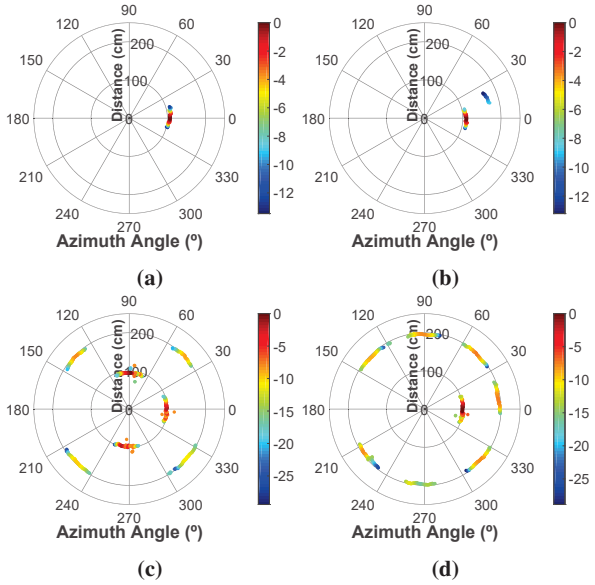

Figure 5. Polar PPI: Normalised gain (in dB) *vs.* scanning angle, for each experimental scenario: (a) 1-pole (b) 2-pole (c) 7-pole (d) 8-pole.

between the poles (i.e. 1.2 m), in addition reflection loss introduced by the second pole (i.e around 2 dB).

4 Conclusions

This paper presents the first results on STDCC radar based on PN sequences. The radar architecture including baseband generation, RF front-end and IF stage are detailed in this manuscript. Subsequently, experimental results performed inside an anechoic chamber are presented and discussed. Four distinct scenarios have been considered by disposing multiple artificial targets at different locations around the radar sensor. The proposed radar not only successfully detected and the targets on multi-clutter environment but also accurately identified the absolute position (distance and angle from boresight) of each target, with a range error of only 9 cm, which falls within the radar resolution. This results prove and validate the usefulness of the STDCC technique applied in radar, representing a quantum leap in radar future front-end architecture.

5 Acknowledgements

This work is partially funded by Research and Technological Development Incentive Scheme CO-PROMOTION - Centro2020 - P2020 - European Regional Development Funds, under project RADAVANT - Radar for Detection and Avoidance in Unmanned Aerial Vehicles (PI nr. 033907) and by FCT/MCTES UIDB/EEA/50008/2020.

References

[1] W.Wiesbeck and L. Sit, "Radar 2020: The future of radar systems," *International Radar Conference*, pp. 1–6, Oct. 2014.

[2] J. S. A. Gameiro, D. Castanheira and P. P. Monteiro, "Research Challenges, Trends and Applications for Future Joint Radar Communications Systems," *Wireless Personal Communications*, vol. 100, no. 1, pp. 81–96, May 2018.

[3] R. J. Pirkl and G. D. Durgin, "Optimal Sliding Correlator Channel Sounder Design," *IEEE Transactions on Wireless Communications*, vol. 7, no. 9, pp. 3488–3497, Sep. 2008.

[4] D. Ferreira, R. F. S. Caldeirinha, and N. Leonor, "Real-time High-resolution Radio Frequency Channel Sounder Based on the Sliding Correlation Principle," *IET Microwaves, Antennas Propagation*, vol. 9, no. 8, pp. 837–846, 2015.

[5] R. Feger, H. Haderer, H. Jalli Ng, and A. Stelzer, "Realization of a Sliding-Correlator-Based Continuous-Wave Pseudorandom Binary Phase-Coded Radar Operating in W-Band," *IEEE Transactions on Microwave Theory and Techniques*, vol. 64, no. 10, pp. 3302–3318, Oct 2016.

[6] R. F. S. Caldeirinha, J. R. Reis, A. Sardo, L. Duarte, N. Leonor, J. Gil, and C. Ribeiro, "Disruptive future of radar based on all-digital PN signal processing," in *2019 IEEE-APS Topical Conference on Antennas and Propagation in Wireless Communications (APWC)*. IEEE, sep 2019.

[7] X. Corporation, "Xilinx Kintex-7 FPGA KC705 Evaluation Kit," 2019. [Online]. Available: https://www.xilinx.com/products/boards-and-kits/ek-k7-kc705-g.html